Modeling betatron radiation using particle-in-cell codes for plasma wakefield accelerator diagnostics

M. Yadav,[1,2,3,*] C. Hansel,[4] B. Naranjo,[1] G. Andonian,[1] P. Manwani,[1] Ö. Apsimon,[5] C. P. Welsch,[2,3] and J. Rosenzweig[1]

[1]*Department of Physics and Astronomy, University of California Los Angeles, Los Angeles, California 90095, USA*
[2]*Department of Physics, University of Liverpool, Liverpool L69 3BX, United Kingdom*
[3]*Cockcroft Institute, Warrington WA4 4AD, United Kingdom*
[4]*Center for Integrated Plasma Studies, Department of Physics, University of Colorado Boulder, Boulder, Colorado 80309, USA*
[5]*Department of Physics and Astronomy, University of Manchester, Manchester M19 3PL, United Kingdom*

(Received 22 August 2024; accepted 23 May 2025; published 7 July 2025)

The analysis of plasma wakefield acceleration experimental measurements, particularly in the characterization of photons emitted through the betatron radiation mechanism, requires the development of accurate numerical models. These computational models are crucial for supporting modern instrumentation designed to measure the single-shot, double-differential angular-energy radiation spectra resulting from interactions between beams and plasmas. Motivated by the needs of such applications, this paper presents detailed numerical models of betatron radiation generated in beam-plasma acceleration experiments. These models are based on the integration of the Liénard-Wiechert (LW) potentials, applied to computed particle trajectories. The particle trajectories are generated using three distinct methods: first, by tracking particles through idealized fields in the blowout regime of PWFA; second, by obtaining trajectories using the fast quasistatic particle-in-cell (PIC) code QuickPIC; and third, obtaining trajectories from the fully self-consistent PIC code OSIRIS. To ensure the accuracy and reliability of these models, the paper includes various benchmark tests using analytical expressions, as well as employing the PIC code EPOCH, which takes an alternative approach by using a Monte Carlo quantum electrodynamics (QED)-based radiation model. Additionally, the paper presents simulations of the expected experimental betatron radiation spectra, taking into account parameters relevant to PWFA and plasma photocathode experiments at the SLAC FACET-II facility.

DOI: 10.1103/ykrl-45h8

I. INTRODUCTION

Beam-driven plasma wakefield accelerators (PWFAs) represent a promising path for achieving high-field acceleration, having already demonstrated acceleration gradients that are orders of magnitude higher than those obtained with conventional radio-frequency acceleration [1]. PWFAs are envisioned as a core technology for next-generation compact, high-energy particle accelerators. In PWFA, a driving electron beam in a plasma excites a wakefield that accelerates a trailing (witness) electron beam. Experiments conducted at the Facility for Advanced Accelerator Experimental Tests (FACET) at SLAC National Accelerator Laboratory [2], the predecessor facility to the current FACET-II, reached several key milestones in realizing practical PWFAs. These milestones include high-efficiency acceleration [3], high total energy gain [4], positron acceleration [5], and the demonstration of a plasma photocathode [6], also known as Trojan Horse injection, a scheme aimed at producing ultra-high-brightness electron beams inside the plasma.

FACET-II is capable of driving electric fields of up to 100 GV/m. Within this accelerator, a 10 GeV electron beam travels through plasma columns ranging from 10 to 30 cm in length, depending on the specific experimental requirements. The plasma density within these columns can vary widely, spanning over 10^{16}–$10^{20}\,\mathrm{cm}^3$, with each density tailored to particular experiments. Some notable experiments planned or underway at FACET-II focus on high-energy electron acceleration in plasma and explore the feasibility and physics potential of this innovative acceleration technique. With a strong emphasis on advancing the understanding of PWFAs to future linear colliders with

*Contact author: yadavmonika@g.ucla.edu

Published by the American Physical Society under the terms of the Creative Commons Attribution 4.0 International license. Further distribution of this work must maintain attribution to the author(s) and the published article's title, journal citation, and DOI.

relevant beam quality, FACET-II seeks to reduce the transverse emittance of the electron beam. In this context, the experimental program requires the development of noninvasive techniques for studying the strongly coupled beam behavior in plasma. Betatron radiation has proven to be an invaluable tool in this regard, offering a single-shot, noninvasive diagnostic method for both laser- or beam-driven plasma accelerators. By measuring the frequency spectrum of betatron radiation, parameters such as the rms transverse beam size can be determined.

Betatron radiation in PWFA [7–9] is produced by the acceleration associated with transverse *betatron* oscillations of charged particles, particularly by electrons influenced by an ion column left bare by the plasma electron response in the PWFA "blowout regime" [10]. Betatron radiation is valuable not only as a carrier of detailed information about beam-plasma interactions but also as a novel radiation source. In this context, we focus on employing betatron radiation as a robust diagnostic tool for both beam and plasma conditions.

The FACET-II facility [11,12] aims to build on previous achievements by demonstrating high beam quality using both externally injected and plasma-injected beams accelerated over significant distances. However, measuring many key characteristics in these experiments is a significant challenge for conventional diagnostics because of factors such as extremely low emittances and small beam sizes. Moreover, the hostile environment through which the beam propagates restricts access to traditional diagnostic methods.

The betatron radiation signal is readily accessible owing to the substantial radiation flux produced by relativistic beams within plasma fields. Betatron radiation diagnostics have been employed in inverse Compton scattering experiments [13] and studied in proton-driven PWFA experiments at AWAKE [14]. While the implementation of betatron radiation diagnostics has been attempted at FACET, the high emittance of the beams resulted in degraded emitted radiation spectra, limiting their full potential. With improved beam condition at FACET-II, the betatron diagnostic system is expected to provide both angular and radiation spectral information about the emitted betatron radiation on a shot-by-shot basis, yielding essential insights into the plasma-accelerated beam.

In such challenging circumstances, advanced machine learning (ML) methods [15–17] prove to be valuable for predicting the longitudinal phase space, nondestructive interference of transverse beam emittance, and radiation spectral reconstruction of the bunch profile. However, electron beam facilities will need to rely on betatron radiation as a critical mechanism to enhance diagnostic capabilities since betatron radiation provides a nondestructive measurement approach that takes advantage of the strong beam focusing in plasma.

Betatron radiation models should generate large datasets for ML-based models, or this information can be used in conjunction with a maximum likelihood estimation (MLE) algorithm or similar approaches. Recent work [18,19] has utilized data from simulated PWFA experiments to yield betatron radiation spectra that reliably reconstruct beam parameters using ML methods. The betatron radiation spectrum in this preliminary analysis extends beyond 100 MeV in very high plasma density scenarios. Studies on changes in the nominal emitted betatron spectrum because of beam-plasma instabilities are now underway, emphasizing the need for predictive models to interpret the experimental signals under such conditions.

Among various numerical techniques, PIC codes [20] are suitable for computing the motion of charged particles in a plasma environment. These codes excel in simulating complex systems where the interactions between charged particles and electromagnetic fields are nonlinear and dynamic, making them indispensable in studying beam-plasma interactions. This work discusses novel radiation algorithms to study the radiation emitted by beam-plasma interactions. Various techniques are available for computing the motion of charged particles. Analytical methods involve mathematically modeling the motion of charged particles using predetermined equations of motion and solving them analytically. Numerical integration techniques, such as the Runge-Kutta method, are used to compute particle trajectories step by step. Computational approaches often rely on approximate or self-consistent PIC codes to extract information about particle trajectories. Additionally, statistical methods like the Monte Carlo simulations model the motion of charged particles by randomly sampling their path through space and averaging results over multiple simulation runs.

In this paper, we introduce numerical models for computing betatron radiation spectra from PWFAs and plasma injection scenarios. These models can be used to reconstruct beam parameters from betatron radiation signatures. In our approach, radiation is computed by integrating Liénard-Wiechert (LW) potentials for particle trajectories obtained using different PIC codes. The radiation spectra from different models are validated, compared, and used to simulate expected radiation properties in upcoming PWFA and plasma injection experiments at FACET-II. Spatial and temporal profiles of radiation are also important for studying the orbital angular momentum of light, which may be obtained through helical motion permitted by the beam-plasma interaction [21].

The primary focus is on PWFAs, which have the potential to revolutionize particle accelerators by enabling high-gradient acceleration. The research also involves numerical modeling to gain deeper insights into the behavior of intense electron beams within the plasma and the application of machine learning to reconstruct beam parameters. Additionally, advanced photon spectrometers, such as Compton and pair spectrometers, are designed to measure emitted radiation across a variety of experimental scenarios. Despite these promising advancements, the research faces challenges. These challenges

include the computational complexity of modeling beam-plasma interactions, technical obstacles related to betatron radiation measurements, and unaddressed scenarios such as beam misalignment and instabilities. Nonetheless, this work contributes significantly to a deeper understanding of beam-plasma interactions and enhances the accuracy of beam diagnostics within the context of PWFAs.

This paper is organized as follows: In Sec. II, we present a brief analytical description of betatron radiation generated by a Gaussian beam in an ion channel. In Sec. III, we discuss numerical models for betatron radiation from plasma-accelerated beams, computed using various PIC codes. In Secs. III C and III D, we present simulations of planned PWFA and plasma injection experiments, respectively, and discuss the expected general features of the radiation. Finally, in Sec. IV, we conclude by presenting a combined numerical model of betatron radiation generation and its appearance in betatron radiation diagnostics.

II. ANALYTIC DESCRIPTION OF THE RADIATION SPECTRUM

We begin by deriving the single-particle spectrum for an idealized picture of the charged particle motion and then extend this model to describe the spectrum of a particle distribution. In the blowout regime, the drive beam leaves behind an ion channel, which can be assumed to be uniform provided that ion motion [10,22] is insignificant. In the case of paraxial ($\boldsymbol{p}_\perp \ll p_z$) motion, beam electrons undergo simple harmonic motion with an angular (betatron) wave number, $k_\beta = k_p/\sqrt{2\gamma}$, where γ is the Lorentz factor, $k_p = \sqrt{4\pi r_e n_0} = \omega_p/c$ is the plasma wave number, n_0 is the plasma density, and r_e is the classical electron radius [9]. Beam electrons emit undulator radiation characterized by an equivalent undulator strength parameter $K = \gamma k_\beta r_\beta$, where r_β is the particle's maximum transverse excursion during its oscillation.

In the ion channel, each particle in a paraxial beam has a different value of K, depending on the oscillation amplitude. In contrast to undulator radiation, where K is constant in the periodic dipole field array, the radiation spectra of PWFA betatron radiation can be different for varying maximum offsets. The radiation spectrum encompasses different amplitude-dependent regimes, which are categorized into three undulator regimes [8]. For $K \ll 1$, radiation is emitted in a cone containing angles $\theta \lesssim 1/\gamma$, where θ is the radiation's relativistic cone opening angle. The radiation spectrum is sharply peaked around the total photon energy $\epsilon_1 = 2\hbar c\gamma^2 k_\beta/(1+\gamma^2\theta^2+K^2/2)$. When the undulator parameter increases to, e.g., $K \sim 1$, integer harmonics of the fundamental begin to be generated, and the radiation is emitted in a broadened cone containing angles $\theta \lesssim K/\gamma$. As K increases, more harmonics are produced, leading to a greater angular spread. For $K \gg 1$, the harmonics blend to form a smooth, synchrotron-radiation-like spectrum characterized by the familiar critical photon energy $\epsilon_c = 3\hbar cK\gamma^2 k_\beta/2$.

The radiation spectra produced by a single particle are described by these three regimes. To determine the total radiation emitted by the electron beam, we integrate over a range of K values for a given beam distribution. Given that the beam spot size $\sigma_r \gg 1/(\gamma k_\beta)$, most particles in the beam produce radiation in the $K \gg 1$ regime. Since these particles generate significantly more photons than those with small K, the overall radiation emitted by the beam is dominated by the large amplitude particles.

The radiation from a single particle in the $K \gg 1$ regime, assuming no $\hat{z}$ angular momentum component, is given by the following equation:

$$\left(\frac{dI}{d\epsilon}\right)_{\mathrm{sp}} = \frac{I_{\mathrm{tot,sp}}}{\epsilon_{c,\mathrm{sp}}} S_{\mathrm{sp}}\left(\frac{\epsilon}{\epsilon_{c,\mathrm{sp}}}\right), \tag{1}$$

where $\epsilon_{c,\mathrm{sp}}$ and $I_{\mathrm{tot,sp}}$ are the critical photon energy and total radiated energy by a single particle, respectively, which is given by [7]

$$I_{\mathrm{tot,sp}} = \frac{1}{6} r_e m_e c^2 k_p^4 L_p \gamma^2 r_\beta^2, \tag{2}$$

$$\epsilon_{c,\mathrm{sp}} = \frac{3}{4}\hbar c k_p^2 \gamma^2 r_\beta, \tag{3}$$

and

$$S_{\mathrm{sp}}(x) = \frac{9\sqrt{3}}{8\pi} x \int_x^\infty K_{5/3}(y)\,\mathrm{d}y, \tag{4}$$

where K is a Bessel function and L_p is the plasma length. The function $S_{\mathrm{sp}}(x)$ is a synchrotron radiation function [8], satisfying the normalization condition $\int_0^\infty S_{\mathrm{sp}}(x)dx = 1$. Integrating the single-particle spectrum over the beam distribution yields the total radiation spectrum produced by the beam. In the case of a monochromatic Gaussian beam, the spectrum is given by

$$\begin{aligned}\left(\frac{\mathrm{d}I}{\mathrm{d}\epsilon}\right)_b &= 2\pi \int_0^\infty \left(\frac{\mathrm{d}I}{\mathrm{d}\epsilon}\right)_{\mathrm{sp}} \frac{Q}{2\pi\sigma_\perp^2 e} e^{-\frac{r_\beta^2}{2\sigma_\perp^2}} r_\beta dr_\beta \\ &= \frac{I_{\mathrm{tot},b}}{\epsilon_{c,b}} S_b\left(\frac{\epsilon}{\epsilon_{c,b}}\right),\end{aligned} \tag{5}$$

where Q is the total beam charge, and $\sigma_\perp$ is the average radius of the beam particles,

$$S_b(x) = \frac{9\sqrt{3}\Lambda^4}{16\pi} x^3 \int_0^\infty \int_v^\infty \frac{K_{5/3}(u) e^{-\frac{\Delta^2 x^2}{2v^2}}}{v^3}\,\mathrm{d}u\,\mathrm{d}v, \tag{6}$$

$$I_{\mathrm{tot},b} = \frac{1}{3e} r_e m_e c^2 k_p^4 L_p Q \gamma^2 \sigma_r^2, \tag{7}$$

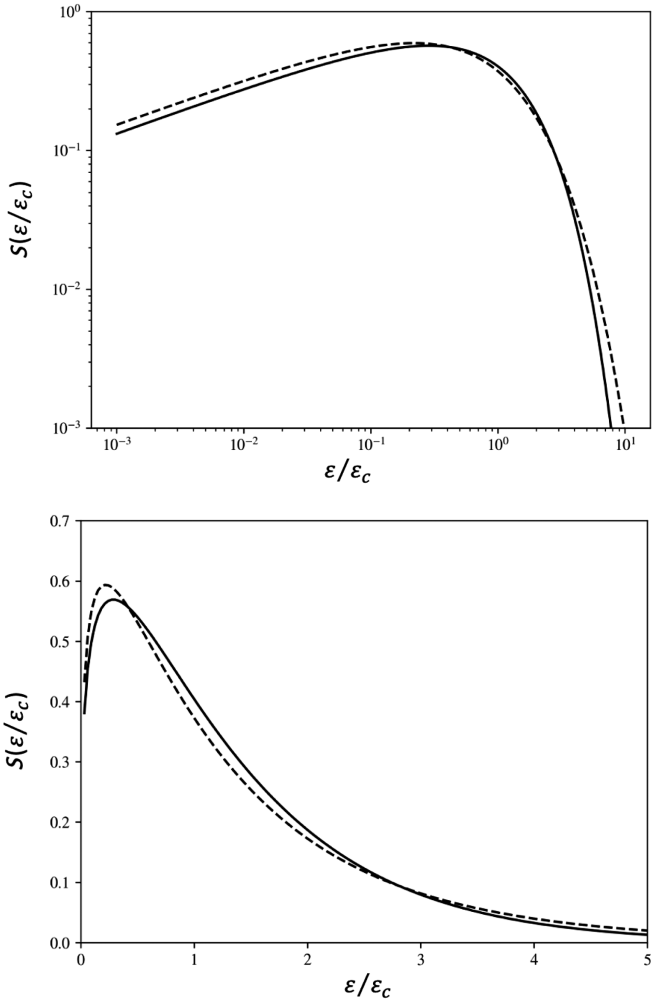


FIG. 1. Normalized analytic betatron radiation spectra as functions of the normalized radiation energy. Solid line: single particle spectrum $S_{\rm sp}(\epsilon/\epsilon_c)$ given by Eq. (4). Dashed line: beam spectrum $S_b(\epsilon/\epsilon_{c,b})$ given by Eq. (6).

and

$$\epsilon_{c,b} = \frac{3}{4}\Lambda\hbar c k_p^2 \gamma^2 \sigma_r. \tag{8}$$

Here Λ is a dimensionless constant determined by the precise definition of the critical energy. We define $S_b(x)$ such that it satisfies the same normalization condition as $S_{\rm sp}(x)$: $\int_0^\infty S_b(x)dx = 1$. The critical energy ϵ_c is defined as the energy at which [23]

$$\int_0^{\epsilon_c} \frac{\mathrm{d}I}{\mathrm{d}\epsilon}\,\mathrm{d}\epsilon = \int_{\epsilon_c}^{\infty} \frac{\mathrm{d}I}{\mathrm{d}\epsilon}\,\mathrm{d}\epsilon. \tag{9}$$

To define $\epsilon_{c,b}$ in a way that fulfills this requirement in the beam case, the constant Λ must in turn satisfy

$$\int_0^\infty \left[1 - e^{-\frac{\Lambda^2}{2x^2}}\left(1 + \frac{\Lambda^2}{2x^2}\right)\right] S(x)\,\mathrm{d}x = \frac{1}{2}. \tag{10}$$

Numerically evaluating this gives $\Lambda \approx 1.7231$. A plot of $S_{\rm sp}(x)$ and $S_b(x)$ is shown in Fig. 1. The plot highlights that the overall shape of the normalized single-particle and beam radiation spectra, $S_{\rm sp}(x)$ and $S_b(x)$, is similar.

However, it is important to note that these equations provide a simplified model that does not account for many of the important effects that may influence betatron radiation, such as acceleration, energy spread, $\hat{z}$ angular momentum of beam electrons, plasma ramps, and the contribution of low K core of the beam.

III. NUMERICAL MODELS OF BETATRON RADIATION

This section introduces three numerical models for computing betatron radiation at three increasing levels of fidelity and computational cost. When using PIC codes to capture short wavelength radiation, there is a trade-off involved in terms of computational resources because of the need for higher grid resolution.

A. Idealized particle tracker with Liénard–Wiechert radiation

We have developed a betatron radiation code that tracks particles as they move through plasma wakefields and computes the emission of electromagnetic radiation by these charged particles undergoing the resultant idealized betatron oscillations. The code is implemented in C++ and parallelized using Boost.MPI, enabling large-scale simulations.

In the first step of our simulation approach, we randomly sample macroparticles from a Gaussian beam distribution. To approximate their behavior within the PWFA blowout regime, these particles are tracked through idealized acceleration and focusing fields. We employ a fourth-order Runge-Kutta (RK4) integration method for this purpose. Specifically, the fields used include a focusing force that is linear in r, arising from the nominally uniform ion channel, and a constant accelerating field, represented as $\boldsymbol{E} = Z_i m_e \omega_p^2 \boldsymbol{r}_\perp/2e + E_{\rm accel}\hat{\boldsymbol{z}}$, where $E_{\rm accel}$ is an input parameter. The electron trajectories are used to numerically integrate the complex LW potential for each particle. The LW potential for particle i is given by the equation:

$$\boldsymbol{V}_i = \int_{t_i}^{t_f} \frac{\boldsymbol{n} \times [(\boldsymbol{n} - \boldsymbol{\beta}) \times \dot{\boldsymbol{\beta}}]}{(1 - \boldsymbol{n}\cdot\boldsymbol{\beta})^2} e^{\frac{i\epsilon}{\hbar}[t - \boldsymbol{n}\cdot\boldsymbol{r}(t)/c]}\,\mathrm{d}t, \tag{11}$$

where $\boldsymbol{n}$ is the unit vector in the direction of radiation observation, $\boldsymbol{\beta}$ represents the velocity of the electron normalized to the speed of light c. Thus, $\dot{\boldsymbol{\beta}}$ represents the acceleration divided by c, and ϵ is the photon energy. The quantity $\boldsymbol{V}_i$ is computed over a 3D grid spanning different directions and photon energies. This computation takes place simultaneously with particle tracking, and the particle data do not need to be saved; it can be discarded after being used to compute its contribution to the fields. Each message

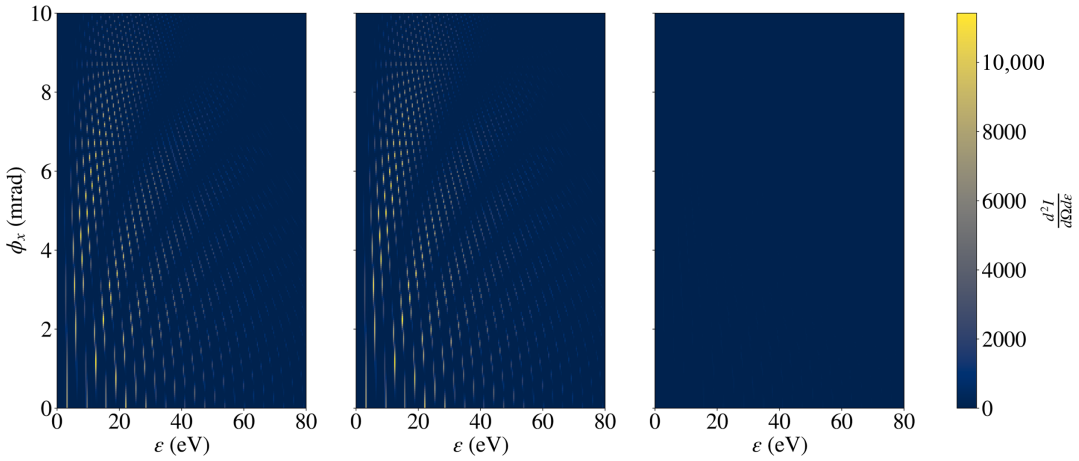


FIG. 2. Double differential spectra for the second benchmark of the model discussed in Sec. III A. Left: analytical spectrum. Middle: spectrum computed by the model. Right: absolute error between the two radiation spectra.

passing interface (MPI) process computes its contribution to the radiation independently and in parallel, and the contributions are summed at the end of the computation.

Consequently, the double differential spectrum is given by

$$\frac{d^2I}{d\Omega d\epsilon} = \frac{e^2}{16\pi^3\epsilon_0\hbar c}\left|\sum_i w_i \boldsymbol{V}_i\right|^2, \tag{12}$$

where $w_i \equiv \sqrt{|Q_{i,\mathrm{mp}}|/e}$ represents the particle's weight. The primary bottleneck in this calculation is the $O(N^3)$ scaling of the 3D grid resolution and the small time step required to prevent aliasing, particularly high photon energies ϵ. While the number of simulated particles is typically small—even with just a few hundred—the statistical error in the computed radiation spectrum tends to remain acceptably low.

TABLE I. Parameters for the second benchmark simulation for the idealized particle tracker and LW.

Parameter	Value	Unit
Plasma density	4×10^{16}	cm^{-3}
Plasma length	60	cm
Beam energy	10	GeV
Beam charge	500	pC
Beam spot size	4.5	μm
Beam normalized emittance	0 or 75[a]	mm mrad
Simulation particles	500	
Step size	12	μm
$\phi_{x,y}$ window	$[-1.5, 1.5]$	mrad
$\phi_{x,y}$ points	51	
ϵ range	[0.5, 5000]	keV
ϵ points	101	
ϵ spacing	Logarithmic	

[a]Two simulations were conducted, one with zero emittance and one with matched emittance.

We performed two benchmark tests to validate the code. In the first test, we tracked a single particle through an ion channel. This particle had an energy of $E = 100$ MeV, an equivalent undulator parameter $K = 2$, and a betatron period of $\lambda_\beta = 1$ cm. It was tracked for 10 betatron periods with 100 steps per period. The analytical and numerical double differential spectra and the absolute error between them are shown in Fig. 2, demonstrating good agreement between simulation and theory.

For the second benchmark, we tracked a beam with parameters based on PWFA experimental plans at FACET-II, as shown in Table I. Two simulations were performed—one with zero emittance and one with finite emittance. The spot size was chosen so that the beam was matched to the plasma focusing, using the relation $\sigma_r^2 = \epsilon/\gamma k_\beta$. The radiation spectra from both of these simulations are compared to the analytic expression from Eq. (5) in Fig. 3.

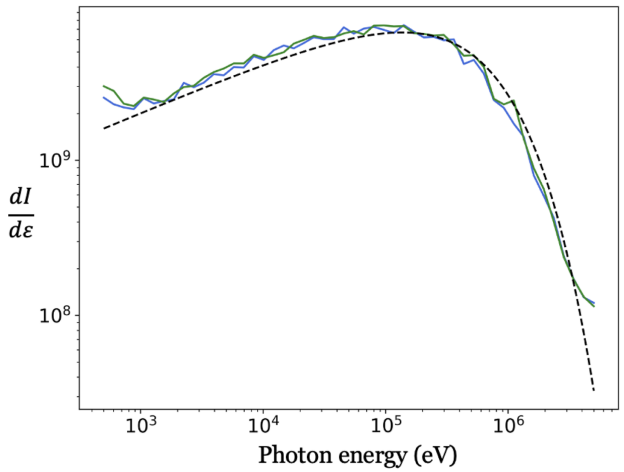


FIG. 3. Synchrotron radiation spectra for the second benchmark of the model discussed in Sec. III A. Blue: simulation with zero emittance. Green: simulation with matched emittance. Black, dashed: analytic spectrum.

B. Quasistatic particle-in-cell simulations with Liénard–Wiechert radiation

At the next level of sophistication, we utilized a 3D quasistatic PIC code, QuickPIC [24,25], to compute betatron radiation. Quasistatic PIC codes use the approximation that the beam evolves on a much slower timescale than the plasma response to the beam. This approximation enables significant speedups over conventional PIC codes and is particularly accurate when simulating PWFA. However, it limits the applicability of quasistatic codes to scenarios where fast-changing beam phenomena, such as plasma injection with attendant nonrelativistic beam motion, are not important.

Compared to the model discussed in Sec. III A, the numerical model derived from the quasistatic code can accurately describe the radiation from the PWFA drive beam, even when it is only partially inside the ion channel. It can also capture the radiation signature of effects caused by instabilities such as hosing, which has a notably longer length scale than λ_p. Although QuickPIC does not directly compute radiation, we modified it to output beam-particle trajectory information. We then selected a random subset of these particles and used them as input for a code based on the LW calculation method discussed in Sec. III A. This approach is similar to the method used in [26] to compute betatron radiation.

With the LW potential integral described in Eq. (11), accurately computing high-energy radiation without aliasing effects requires a very small step size. This step size is typically notably smaller than the step size needed to track particle motion during the oscillation.

TABLE II. Parameters for Sec. III B benchmark simulation.

Parameter	Value (drive, witness)	Unit
Plasma density	4×10^{16}	cm^{-3}
Plasma length	60	cm
Plasma radius	31.9	μm
Beam energy	10, 10	GeV
Beam charge	500, 500	pC
Beam spot size	5, 4.5	μm
Beam length	5, 2.8	μm
Beam normalized emittance	3.2, 3	mm-mrad
Beam separation	101.55	μm
QuickPIC resolution	$1.04 \times 1.04 \times 0.60$	μm
QuickPIC time step	1.10	ps
QuickPIC macroparticles	64^3	
LW particles	100	
LW time step	66.7	fs
LW angular window	$[-1, 1]$	mrad
LW angular grid points	25×25	
LW angular grid spacing	Linear	
LW energy window	$[5 \times 10^3, 5 \times 10^6]$	eV
LW energy grid points	50	
LW energy grid spacing	Logarithmic	

To address this requirement, we interpolate additional trajectory points between those computed by QuickPIC, using cubic B-spline interpolation. This was not done in Sec. III A because the speed of the simple RK4 tracker in Sec. III A allowed particles to be tracked with smaller steps than necessary without significantly increasing computation time. Additionally, in this section, the LW code used the Python `multiprocessing` module and computed the radiation only after the particle tracking step was completed.

To benchmark this approach against Eq. (5), we used the parameter set shown in Table II. To enable benchmarking, this parameter set minimizes witness beam acceleration by placing it at the zero crossing of the longitudinal wakefield. We computed radiation from the witness beam, with the time evolution of the drive beam turned off. The computed spectrum, displayed in Fig. 4, aligns well with the theoretically predicted spectrum.

C. OSIRIS full particle-in-cell code with Liénard–Wiechert radiation

We now turn to the most sophisticated approach, which is required for analyzing complex scenarios such as plasma-based injection using the Trojan Horse mechanism. In the Trojan Horse plasma photocathode scheme, the initially neutral species comprise both a high ionization threshold (HIT) gas and a low ionization threshold (LIT) gas. The LIT gas is laser-pre-ionized, and the passage of the drive beam creates a strong plasma wave blowout. Within this blowout, another laser is used to inject electrons released from the HIT gas. To simulate the FACET-II Trojan Horse experimental scenario, we require a more advanced code and, thus, we employed the OSIRIS code for this purpose. The OSIRIS simulations primarily focused on generating the witness beam using the collinear laser

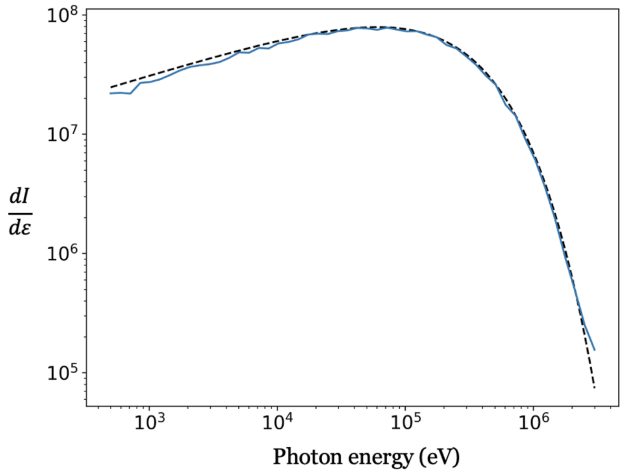


FIG. 4. Blue: radiation spectrum computed numerically using the method discussed in Sec. III B. Black, dashed: analytical radiation spectrum based on Eq. (5).

TABLE III. Laser and electron beam parameters for Trojan Horse experiment at FACET-II.

Parameter	Value
Species	H
Laser wavelength (nm)	800
Tau (fs)	50
Laser a_0	0.02
Plasma wavelength (μm)	250
$nH2(\mathrm{LIT}) = nHe(\mathrm{HIT})\ (\mathrm{cm}^{-3})$	1.789×10^{16}
$n_0\ (\mathrm{cm}^{-3})$	1.79×10^{16}
ω_p (μm)	100
k_p^{-1} (μm)	39.79
Beam peak density	$9.3 \times 10^{23} = 52$
Drive beam parameter	Unit
E (GeV)	10
Q (nC)	−1.5
$Qtilda$	8.3
Ω_l	313
N	3.1×10^9
Laser beam waist (μm)	7
$\sigma_x$unmatched (μm)	4.5
$\sigma_y$unmatched (μm)	4.5
σ_z (μm)	12.15
$\epsilon_{n,x}$ (μm)	5
$\epsilon_{n,y}$ (μm)	5

ionization injection scheme. Ultimately, we utilized this simulation approach to calculate betatron radiation by importing trajectories obtained from OSIRIS into the LW model.

We implemented a plasma profile that consists of a vacuum section followed by a short ramp of increasing density to match the desired experimental scenario. The zero-density section was included to initialize a laser pulse, ensuring the consistency between the simulation and the local validity of the Maxwell equations. A 3D Gaussian laser pulse is used in OSIRIS, with leading-order corrections applied to the longitudinal electric field to account for beam expansion because of diffraction and the short pulse duration. The model features control over parameters such as focal spot position, temporal pulse center, and longitudinal magnetic fields for out-of-plane laser polarization.

The simulated scenario used an 800 nm laser with a spot size of a few μm that was initiated in the zero-density region with a normalized vector potential value of $a_0 = 0.02$ (Table III). The chosen spot size ensures sufficiently large field regions for the probe beam injection. The plasma channel had a width of 250 μm and a plasma density of $1.79 \times 10^{22}\ \mathrm{m}^{-3}$, ensuring a nearly constant laser spot size during propagation, with a 30 cm long dephasing length matching the anticipated plasma length for the future experimental studies. In experimental setups, a cryogenically cooled gas jet operating at several atmospheres of pressure can be used to generate the necessary density profile [27]. The laser used to ionize the HIT gas, which provides injection, is locally within the blowout region. The electrons created are captured and accelerated to relativistic energies by the strong electric fields associated with the plasma wake.

A 1.5 nC electron drive beam with a $\gamma = 20,000$, a matched spot size of approximately ∼1 μm and a longitudinal length of 12.15 μm is simulated. The laser-induced injection phase is determined such that minimal accelerating field acts on the probe beam, while the focusing fields are at their nominal maximum values. The transverse (E_r and B_θ) and longitudinal wakefields (E_x), are self-consistently related through the constraints of the Panofsky-Wenzel theorem [28]. We note that this study, to be implemented at FACET-II, builds off the first successful demonstration of plasma photocathode at FACET [6]. In a major improvement over this initial study, the experiment involves an ionization laser pulse injected collinearly, rather than perpendicularly, as in the previous experiment, to generate ultracold electron beams. This innovation enabled the generation of ultralow emittance electron beams capable of driving x-ray-free electron lasers with high brightness and coherence on a femtosecond timescale [29].

There are unique challenges involved in simulating betatron radiation emission processes for this experiment. The quasistatic PIC code used in model, discussed in Sec. III B, cannot simulate beam ionization. Furthermore, achieving the required resolution using the EPOCH code would require computational resources exceeding current capabilities.

In this experiment, the achievable normalized emittance for the witness beam is predicted to be well below the (μrad) scale. Physical effects limiting this performance are inherent in the injection process. This process includes the initial release of He-derived HIT electrons by the laser pulse, which forms the trapped witness bunch. The oscillating fields of the laser pulse can ionize both LIT and HIT gas media at intensities orders of magnitude below those needed to drive plasma waves; these fields are thus perturbative to plasma bulk motion. In the FACET-II experiment, the Ti: Sapphire plasma photocathode ionization laser pulse with a fsec duration is, as noted above, aligned collinearly with the propagation axis of the electron bunch driver. It initially trails the electron bunch at a distance of a few μm behind the driver but gradually moves forward in the bunch frame.

Trojan Horse injection is effectively employed to enhance the electron beam quality and brightness, producing a witness bunch with higher phase-space quality than that of the driver. The radiation spectra from the witness beam differ from those of the driver in many ways, particularly in energy and betatron amplitudes. In this regard, we note that the radiation may be tailored by enhancing the betatron oscillations through the off-axis release of HIT electrons.

For nominally ideal injection, the goals, in general, are to optimize witness bunch compactness, charge, and

emittance. The characteristics of the electron bunch driver are important only as they impact the excitation of the wakefield. Many diagnostic systems needed for characterizing the electron beam will be available at FACET-II. These include, most relevantly to this discussion, betatron radiation spectrum measurement via a Compton spectrometer. Beyond this, downstream beam imaging systems and momentum-resolving spectrometers can assess the phase-space dilution of accelerated beams.

The Compton spectrometer enables double-differential (energy-angle) spectrum measurement. Radiation analysis for the Trojan Horse is complicated because the generated witness beam will generally be of lower energy, and the radiation generated overlaps with the intense driver spectrum at low energy. The spectrometer's angular resolution capabilities are, therefore, critically important, as angular-dependent radiation diagnostics can separate the drive and witness radiation spectra.

For this experimental scenario, OSIRIS [30] was used to simulate particle trajectories. These trajectories were fed into the same LW code used with QuickPIC. Sampling particles from OSIRIS was more complex than sampling from QuickPIC because the former has variable-weighted particles, while the latter uses uniform particle weights. Furthermore, the version of OSIRIS used lacks built-in sampling functionality.

To correctly sample, an initial simulation was performed in which all the particles and weights were dumped. However, only a few output files were generated to prevent disk-write bottlenecks and the creation of unmanageably large data files. Next, particles are sampled with replacement, where the probability of sampling particle i is given by $p_i = w_i / \sum_j w_j$, where w_i is the weight of the ith particle. After particle sampling, redundant particles were consolidated by summing their weights. After this, a second simulation is run where the OSIRIS input file instructs the code to only output particles with IDs in the list of sampled particles. Trajectories were computed from the output files, and the LW integral was computed using Eqs. (11) and (12), where the $\boldsymbol{V}_i$ are scaled by the square root of the particle weights.

In OSIRIS 3D PIC code, the electromagnetic field diagnostics can only be done when species are present. For the betatron radiation generated in the system, we ran the same simulation twice, first by keeping the tags on and then tracking those tags for a longer duration; the schematic is shown in Fig. 5. Tracks specify the frequency at which particle tracking information is written to file. Plasma particle tracking is also used for spectrum. Particle tracking in PIC codes usually involves two steps. In the first step, the simulation is performed, and the information for all the particles is stored at a given time step. With this information, data mining of the relevant particles to be tracked can be performed, e.g., by selecting particles in a given region of phase space. The information of the tags of the particles to be followed can then be saved, and this information is then used as input for a second simulation, identical to the first simulation, where the tracks for the selected particles are going to be saved. The radiation diagnostic uses information from particle trajectories, position, and momentum over time to determine the energy radiated by an accelerated charged particle. All the values for particles whose tags are in the file tags file will be saved to memory every n iteration, tracking timesteps.

In Fig. 6, synchrotron radiation spectra for the driver beam are shown, and the spectrum is narrow. OSIRIS is already a benchmark with other PIC codes. It is worth noticing that the recently published [31] algorithm characterizes the electromagnetic waves in simulations using LW potentials to extract radiation emission and our model's results are in agreement with the OSIRIS radio code.

D. Benchmarking using particle-in-cell code EPOCH with Monte Carlo QED radiation approach

Despite the advanced capabilities of the PIC and LW radiation models, certain effects require a higher-level treatment to be accurately simulated. Monte Carlo QED radiation models handle high-energy photons as discrete particles, calculating their emission probability within the simulation, given the electron motion. This approach is especially valuable when dealing with extremely high electron energies and allows for the inclusion of quantum recoil and strong field effects. One example of such an



FIG. 5. Schematic of OSIRIS radiation code. Stepwise illustration of the position and momentum to track the particles.

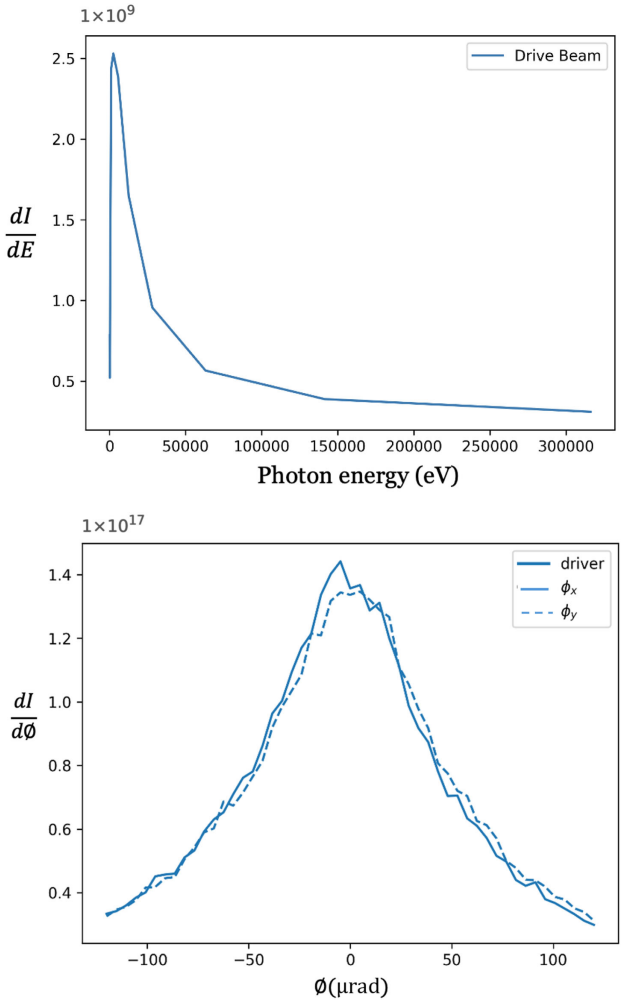


FIG. 6. Top: photon energy spectrum of the radiation emitted by the driver bunch computed using OSIRIS and LW code. Bottom: 1D angular distribution of betatron radiation generated by the driver beam, represented by ϕ_x and ϕ_y.

approach is the EPOCH code, a fully explicit 3D PIC code that employs a Monte Carlo QED model for radiation generation [32,33].

However, we encounter computational limitations when attempting to accurately simulate radiation using this method. A primary challenge with 3D explicit codes is the artificial slowdown of the speed of light on a finite-difference time-domain (FDTD) grid. This effect causes relativistic electrons to nonphysically emit numerical Cerenkov radiation (NCR) at wavelengths near the grid cell size [34]. To mitigate this issue, EPOCH utilizes a dispersion-reduced FDTD solver [35] and an eight-point compensated [36] linear current filter. These schemes help reduce NCR and other instabilities, but they may slightly alter the Fourier content of fields near the grid resolution. It is important to note that the radiation model in EPOCH is photon based, not field based, and the emitted radiation wavelengths can, therefore, extend well beyond the grid resolution.

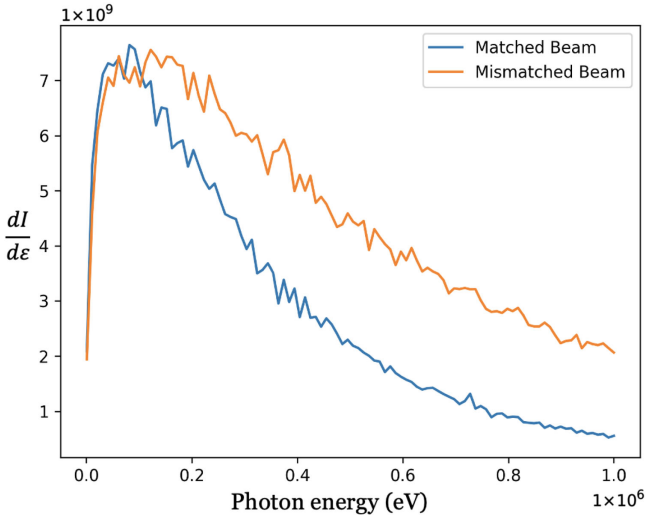


FIG. 7. Photon energy spectrum of the radiation emitted by the driver bunch computed using EPOCH code for matched and mismatched beam at the plasma entrance.

Thus, we expect minimal interference from the smoothing filter and dispersion effects on our results while retaining the benefit of smooth fields for use in QED calculations. A significant challenge when using EPOCH is that extensive computational resources are required to resolve physically relevant length scales, especially in cases where the beam spot size is very small, as in a matched system at FACET-II. In the simulations, we set up a domain with $512 \times 512 \times 512$ cells in all directions to ensure minor features could be resolved. Both drive and witness beams in the plasma are represented by numerous macroparticles per cell, assuming immobile neutralizing background ions.

In EPOCH, a smoothing function is applied to the current generated during the particle push, helping to reduce self-heating and noise in a simulation. This smoothing function can be fine-tuned to suppress high frequencies in the currents and mitigate the effects of NCR. With current filtering enabled, various smoothing functions can be applied to optimize both simulation speed and accuracy.

As shown in Fig. 7, we used EPOCH to simulate an electron beam matched or mismatched to the blowout plasma channel. In the mismatched case, larger oscillation amplitudes in the beam envelope and trajectories lead to higher photon energies. EPOCH's ability to capture the high-energy end of the spectrum is a key advantage.

IV. CONCLUSION

In this paper, an investigation of the motion of charged particles in plasma and the resultant betatron radiation emitted has been carried out. This analysis has employed a comprehensive array of techniques, including analytical methods, numerical methods, PIC methods, Monte Carlo simulations, and hybrid methods. By combining these techniques, the study leveraged their respective strengths

and addressed the limitations of individual codes. Key comparisons and validations were made against analytical expressions under specific conditions, accounting for both vanishing and finite parameters, including matched spot size. Benchmarking to analytical models was performed by minimizing witness beam acceleration and suppressing the time evolution of the drive beam.

This study highlights the suitability of the model discussed in Sec. III A for handling large datasets, while the model in Sec. III B has proven efficient for FACET-II-related experiments and other beam-driven plasma physics because of its computational efficiency. The approach in Sec. III C extended the analysis by calculating radiation through trajectories obtained from the full PIC code OSIRIS. Further benchmarks were conducted using the LW-based codes and the EPOCH code, which calculates radiation using QED modules, discussed in the Appendix.

Betatron radiation measurements enable a comprehensive assessment of the radiation spectrum produced by electron beams in beam-plasma interactions, providing an indirect means to measure the beam's phase-space dynamics within the plasma. This knowledge is crucial for optimizing beam dynamics inside a PWFA, particularly in producing high-brightness beams for high-energy physics and light source applications.

Additionally, these measurements can detect deviations from ideal focusing conditions in the plasma, such as those caused by ion collapse, which poses a potential challenge for linear collider beams in a PWFA. Indeed, looking ahead, betatron radiation measurements will be invaluable for diagnosing upcoming experiments at FACET-II involving mobile ions, where a long and intense beam leads to ion column formation. This generates strong focusing fields, resulting in substantial high-energy betatron radiation, serving as a diagnostic tool for understanding beam-plasma interactions. Experiments such as the flat beam-based ion motion experiment at FACET and AWA and the Dragon tail injection experiment will benefit from these diagnostics. Furthermore, recent calculations predict that a high-density, ultrarelativistic electron beam passing through a millimeter-thick conductor can produce bright, collimated gamma-ray pulses with high electron-to-photon energy conversion efficiencies. The E-305 experiment at FACET-II will study this phenomenon, which yields photon energies above 10 MeV, highlighting the importance of advanced diagnostic systems such as Compton spectrometers for future PWFA-based linear collider scenarios.

For the FACET-II PWFA collaboration, the ability to measure beam matching is essential for interpreting the integrated signal and achieving conditions suitable for emittance preservation, the critical goal of this experiment. A strong correlation exists between minimizing emittance growth and reducing the integrated betatron radiation signal, as additional radiation is emitted when the beam is mismatched. In plasma injection experiments with very bright beams, the spectral narrowness of the betatron radiation emissions poses particular challenges, especially in Trojan Horselike scenarios. Robust methods have been developed to invert the observed distribution, as described in [18]. This is accomplished using machine-learning algorithms and MLE methods, with the algorithms identifying established patterns in the data obtained with training information from models such as those presented in this paper. Betatron radiation will also play a significant role in the Dragon tail injection experiment at FACET-II [37]. The slightly off-axis generated witness beam and the driver beam will produce betatron radiation signals, which can be characterized using the above-described models.

Furthermore, radiation diagnostics can be applied to future scenarios involving PWFA-based linear colliders, where highly asymmetric transverse emittances are anticipated. Therefore, betatron radiation diagnostic systems are crucial for characterizing the beam and will be available at FACET-II, with the potential to extend such measurements to even higher energy scales. These approaches include betatron radiation measurements via Compton (discussed above) or pair spectrometers, as described in Refs. [38,39]. These diagnostics complement downstream electron beam measurement systems that assess phase-space dilution of accelerated and decelerated beams, as well as their momentum spectra.

Finally, we note that a fundamental comparison between betatron and undulator radiation is in progress as a part of a UCLA-INFN collaboration. Conventional theories fail to accurately describe the high K and high K/γ regimes, which leads to underestimations of particle trajectory amplitude and period. The insights from this work are crucial for interpreting extreme betatron radiation scenarios, particularly those involved in developing compact, high-brightness radiation sources such as the ion-channel laser.

ACKNOWLEDGMENTS

This work was performed with the support of the U.S. Department of Energy, Division of High Energy Physics, under Contract No. DE-SC0009914 and NSF PHY-1549132 Center from Bright Beams, DARPA under Contract No. HR001120C007 and the STFC Liverpool Centre for Doctoral Training on Data Intensive Science under Grant No. ST/P006752/1. This work used computational services associated with the SCARF cluster, provided by the STFC Scientific Computing Department, United Kingdom.

APPENDIX

1. Benchmarking using full particle-in-cell EPOCH with Monte Carlo QED radiation

Despite the sophistication of the PIC and LW radiation models, some effects still require a higher level of

sophistication to simulate. Monte Carlo QED radiation models treat high-energy photons as discrete particles, and electrons have some probability of emitting them. Statistical properties of the photons could matter, especially at extremely high energies, quantum recoil, statistical properties, and strong field effects. An example is EPOCH, a 3D fully explicit PIC code that uses a Monte Carlo QED model to simulate radiation generation [32,33].

We found that accurately simulating radiation using this method exceeded our computational resources. A primary challenge with 3D explicit codes is the artificial slowdown of the speed of light on a finite-difference time-domain (FDTD) grid. This means, for example, that a relativistic electron propagating along a straight line with constant velocity in free space will nonphysically emit numerical Cerenkov radiation (NCR) at wavelengths corresponding to the grid cell size and may even grow as an instability by imprinting into the current profile [34]. In EPOCH, we use a dispersion-reduced FDTD solver [35] and an eight-point, compensated [36] linear current filter to mitigate this effect. Such schemes are imperfect and can slightly alter the Fourier content of fields at the grid resolution. However, the radiation model in EPOCH is photon based, not field based, and the emitted radiation wavelengths are well beyond the grid resolution. Therefore, we expect minimal interference from the smoothing filter and microscopic details of the dispersion on our results while retaining the benefit of smooth fields to be used in QED calculations. One of the primary challenges associated with using EPOCH is that extensive computational resources are needed to correctly resolve physically relevant length scales, especially in the matched beam case when the beam spot size is small. The domain is set up with $512 \times 512 \times 512$ cells per in the longitudinal and transverse directions, allowing the minor features in those directions to be resolved. Drive and witness beams in the plasma are represented with macroparticles per cell, assuming an immobile neutralizing background.

In Fig. 8, the radiation spectrum is produced using the EPOCH code, the most advanced and computationally demanding betatron radiation model. In EPOCH input files, a smoothing function is applied to the current generated during the particle push. It helps to reduce noise and self-heating in a simulation. It can be substantially tuned to damp high frequencies in the currents and can be used to reduce the effect of NCR. When current filtering is enabled, we can set the following keys: smooth iterations, and integer number of iterations of the smoothing function to be performed. If not present defaults to one iteration, more iterations will produce smoother results but will be slower. Gamma rays emitted from the betatron radiation process in underdense plasma wakefields and high field-laser-induced Compton scattering produce unique experimental signatures that can reveal interaction physics at the challenging ultrashort spatial and temporal experimental scales. Additionally, radiative diagnostics provide a nonintercepting, nondestructive probe of the extreme high-field environments relevant to advanced acceleration techniques.

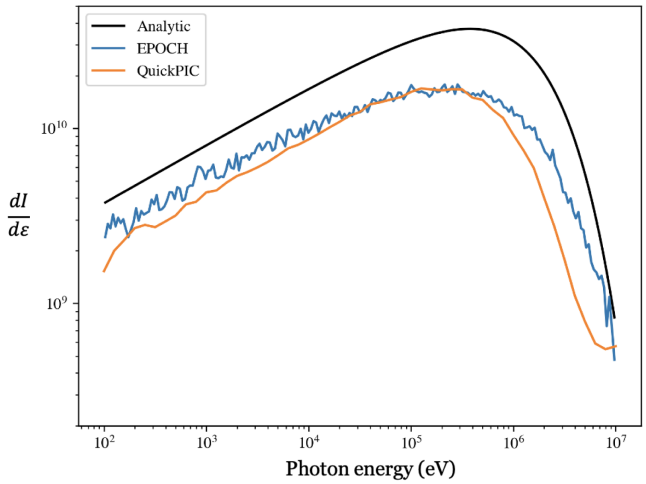


FIG. 8. Benchmark of the photon energy spectrum of the radiation emitted by the driver bunch computed using EPOCH code, analytic and QuickPIC code.

[1] I. Blumenfeld *et al.*, Energy doubling of 42 GeV electrons in a metre-scale plasma wakefield accelerator, Nature (London) **445**, 741 (2007).

[2] M. J. Hogan, T. O. Raubenheimer, A. Seryi, P. Muggli, T. Katsouleas, C. Huang, W. Lu, W. An, K. A. Marsh, W. B. Mori, C. E. Clayton, and C. Joshi, Plasma wakefield acceleration experiments at FACET, New J. Phys. **12**, 055030 (2010).

[3] M. Litos *et al.*, High-efficiency acceleration of an electron beam in a plasma wakefield accelerator, Nature (London) **515**, 92 (2014).

[4] M. Litos, E. Adli, J. M. Allen, W. An, C. I. Clarke, S. Corde, C. E. Clayton, J. Frederico, S. J. Gessner, S. Z. Green, M. J. Hogan, C. Joshi, W. Lu, K. A. Marsh, W. B. Mori, M. Schmeltz, N. Vafaei-Najafabadi, and V. Yakimenko, 9 GeV energy gain in a beam-driven plasma wakefield accelerator, Plasma Phys. Controlled Fusion **58**, 034017 (2016).

[5] S. Corde *et al.*, Multi-gigaelectronvolt acceleration of positrons in a self-loaded plasma wakefield, Nature (London) **524**, 442 (2015).

[6] A. Deng *et al.*, Generation and acceleration of electron bunches from a plasma photocathode, Nat. Phys. **15**, 1156 (2019).

[7] E. Esarey *et al.*, Synchrotron radiation from electron beams in plasma-focusing channels, Phys. Rev. E **65**, 056505 (2002).

[8] S. Corde, K. Ta Phuoc, G. Lambert, R. Fitour, V. Malka, A. Rousse, A. Beck, and E. Lefebvre, Femtosecond x rays from laser-plasma accelerators, Rev. Mod. Phys. **85**, 1 (2013).

[9] I. Kostyukov, S. Kiselev, and A. Pukhov, X-ray generation in an ion channel, Phys. Plasmas **10**, 4818 (2003).

[10] J. B. Rosenzweig, B. Breizman, T. Katsouleas, and J. J. Su, Acceleration and focusing of electrons in two-dimensional nonlinear plasma wake fields, Phys. Rev. A **44**, R6189 (1991).

[11] V. Yakimenko, L. Alsberg, E. Bong, G. Bouchard, C. Clarke, C. Emma, S. Green, C. Hast, M. J. Hogan, J. Seabury, N. Lipkowitz, B. O'Shea, D. Storey, G. White, and G. Yocky, FACET-II facility for advanced accelerator experimental tests, Phys. Rev. Accel. Beams **22**, 101301 (2019).

[12] C. Joshi, E. Adli, W. An, C. E. Clayton, S. Corde, S. Gessner, M. J. Hogan, M. Litos, W. Lu, K. A. Marsh, W. B. Mori, N. Vafaei-Najafabadi, B. O'shea, X. Xu, G. White, and V. Yakimenko, Plasma wakefield acceleration experiments at FACET II, Plasma Phys. Controlled Fusion **60**, 034001 (2018).

[13] Y. Sakai *et al.*, Single shot, double differential spectral measurements of inverse compton scattering in the nonlinear regime, Phys. Rev. Accel. Beams **20**, 060701 (2017).

[14] B. Williamson, G. Xia, S. Gessner, A. Petrenko, J. Farmer, and A. Pukhov, Betatron radiation diagnostics for awake Run 2, Nucl. Instrum. Methods Phys. Res., Sect. A **971**, 164076 (2020).

[15] C. Emma, A. Edelen, M. J. Hogan, B. O'Shea, G. White, and V. Yakimenko, Machine learning-based longitudinal phase space prediction of particle accelerators, Phys. Rev. Accel. Beams **21**, 112802 (2018).

[16] A. Scheinker, S. Gessner, C. Emma, and A. L. Edelen, Adaptive model tuning studies for non-invasive diagnostics and feedback control of plasma wakefield acceleration at FACET-II, Nucl. Instrum. Methods Phys. Res., Sect. A **967**, 163902 (2020).

[17] C. Emma, A. Edelen, A. Hanuka, B. O-Shea, and A. Scheinker, Virtual diagnostic suite for electron beam prediction and control at FACET-II, Information **12**, 61 (2021).

[18] M. Yadav, S. Zhang, M. Oruganti, B. Naranjo, Y. Zhuang, A. Apsimon, C. P. Welsch, and J. B. Rosenzweig, Reconstruction of electron radiation spectra and beam parameters from photon spectrometer data in accelerator experiments using machine learning, Phys. Rev. Accel. Beams **28**, 042802 (2025).

[19] Y. Zhuang, B. Naranjo, J. B. Rosenzweig, and M. Yadav, Spectral reconstruction for FACET-II Compton spectrometer, in *Proceedings of the International Particle Accelerator Conference (IPAC'21), Campinas, SP, Brazil* (JACoW, Geneva, Switzerland, 2021), pp. 4346–4348, 10.18429/JACoW-IPAC2021-THPAB273.

[20] J. M. Dawson, Particle simulation of plasmas, Rev. Mod. Phys. **55**, 403 (1983).

[21] M. Ritsch-Marte, Orbital angular momentum light in microscopy, Phil. Trans. R. Soc. A **375**, 20150437 (2017).

[22] J. B. Rosenzweig, A. M. Cook, A. Scott, M. C. Thompson, and R. B. Yoder, Effects of ion motion in intense beam-driven plasma wakefield accelerators, Phys. Rev. Lett. **95**, 195002 (2005).

[23] A. Hofmann, The physics of synchrotron radiation, in *Cambridge Monographs on Particle Physics, Nuclear Physics and Cosmology* (Cambridge University Press, Cambridge, England, 2004).

[24] C. Huang, V. Decyk, C. Ren, M. Zhou, W. Lu, W. Mori, J. Cooley, T. Antonsen, and T. Katsouleas, QuickPIC: A highly efficient particle-in-cell code for modeling wakefield acceleration in plasmas, J. Comput. Phys. **217**, 658 (2006).

[25] W. An, V. K. Decyk, W. B. Mori, and T. M. Antonsen, An improved iteration loop for the three dimensional quasi-static particle-in-cell algorithm: QuickPIC, J. Comput. Phys. **250**, 165 (2013).

[26] P. S. M. Claveria *et al.*, Betatron radiation and emittance growth in plasma wakefield accelerators, Phil. Trans. R. Soc. A **377**, 20180173 (2019).

[27] E. Parra, S. J. McNaught, and H. M. Milchberg, Characterization of a cryogenic, high-pressure gas jet operated in the droplet regime, Rev. Sci. Instrum. **73**, 468 (2002).

[28] E. Esarey, C. B. Schroeder, and W. P. Leemans, Physics of laser-driven plasma-based electron accelerators, Rev. Mod. Phys. **81**, 1229 (2009).

[29] A. F. Habib, G. G. Manahan, P. Scherkl, T. Heinemann, A. Sutherland, R. Altuiri, B. M. Alotaibi, M. Litos, J. Cary, T. Raubenheimer, E. Hemsing, M. J. Hogan, J. B. Rosenzweig, P. H. Williams, B. W. J. McNeil, and B. Hidding, Attosecond-angstrom free-electron-laser towards the cold beam limit, Nat. Commun. **14**, 1054 (2023).

[30] R. Fonseca *et al.*, OSIRIS: A three-dimensional, fully relativistic particle in cell code for modeling plasma based accelerators, in *Lecture Notes in Computer Science* (Springer Berlin Heidelberg, Berlin, Heidelberg, 2002), pp. 342–351.

[31] M. Pardal, A. Sainte-Marie, A. Reboul-Salze, R. Fonseca, and J. Vieira, Radio: An efficient spatiotemporal radiation diagnostic for particle-in-cell codes, Comput. Phys. Commun. **285**, 108634 (2023).

[32] T. D. Arber, K. Bennett, C. S. Brady, A. Lawrence-Douglas, M. G. Ramsay, N. J. Sircombe, P. Gillies, R. G. Evans, H. Schmitz, A. R. Bell, and C. P. Ridgers, Contemporary particle-in-cell approach to laser-plasma modelling, Plasma Phys. Controlled Fusion **57**, 113001 (2015).

[33] C. Ridgers, J. Kirk, R. Duclous, T. Blackburn, C. Brady, K. Bennett, T. Arber, and A. Bell, Modelling gamma-ray photon emission and pair production in high-intensity laser-matter interactions, J. Comput. Phys. **260**, 273 (2014).

[34] A. D. Greenwood, K. L. Cartwright, J. W. Luginsland, and E. A. Baca, On the elimination of numerical Cerenkov radiation in PIC simulations, J. Comput. Phys. **201**, 665 (2004).

[35] R. Lehe, A. Lifschitz, C. Thaury, V. Malka, and X. Davoine, Numerical growth of emittance in simulations of laser-wakefield acceleration, Phys. Rev. ST Accel. Beams **16**, 021301 (2013).

[36] J.-L. Vay and B. B. Godfrey, Modeling of relativistic plasmas with the particle-in-cell method, C. R. Mec. **342**, 610 (2014).

[37] P. Manwani, D. Bruhwiler, B. Hidding, M. Litos, N. Majernik, and J. Rosenzweig, High brightness electron beams from dragon tail injection and the E-312 experiment at FACET-II, in *Proceedings of the 12th International Particle Accelerator Conference, IPAC-2021, Campinas, SP, Brazil* (JACoW, Geneva, Switzerland, 2021), Vol. 12, pp. 1728–1731, 10.18429/JACoW-IPAC2021-TUPAB146.

[38] B. Naranjo *et al.*, Compton spectrometer for FACET-II, in *Proceedings of the 12th International Particle*

Accelerator Conference, IPAC-2021, Campinas, SP, Brazil (JACoW, Geneva, Switzerland, 2021), Vol. 12, pp. 4332–4335, 10.18429/JACoW-IPAC2021-THPAB269.

[39] B. Naranjo, G. Andonian, N. Cavanagh, A. Di Piazza, A. Fukasawa, E. Gerstmayr, R. Holtzapple, C. Keitel, N. Majernik, S. Meuren, C. Nielsen, M. Oruganti, D. Reis, J. B. Rosenzweig, Y. Sakai, G. Sarri, D. Storey, O. Williams, M. Yadav, and V. Yakimenko, Pair spectrometer for FACET-II, in *Proceedings of the 12th International Particle Accelerator Conference, IPAC-2021, Campinas, SP, Brazil* (JACoW, Geneva, Switzerland, 2021), Vol. 4336.